Enhanced thermopower in the correlated semimetallic phase of hole-doped pyrochlore iridates

R. Kaneko, M.-T. Huebsch, S. Sakai, R. Arita, H. Shinaoka, K. Ueda, Y. Tokura, and J. Fujioka

Phys. Rev. B **99**, 161104 — Published 5 April 2019

DOI: 10.1103/PhysRevB.99.161104

Enhanced thermopower in correlated semimetallic phase of hole-doped pyrochlore iridates

R. Kaneko[1*], M-T. Huebsch[2,3*], S. Sakai[2], R. Arita[1,2], H. Shinaoka[4], K. Ueda[1], Y. Tokura[1,2] and J. Fujioka[1,5,61]

[1] [1] *Department of Applied Physics, University of Tokyo, Hongo, Tokyo 113-8656, Japan*

[2] *RIKEN Center for Emergent Matter Science (CEMS), Wako 351-0198, Japan*

[3] *Graduate School of Frontier Science, University of Tokyo, Kashiwa, Chiba 277-0882, Japan*

[4] *Department of Physics, Saitama University, Saitama 338-8570, Japan*

[5] *Graduate School of Pure and Applied Sciences, University of Tsukuba, 1-1-1 Tennodai, Tsukuba, Ibaraki 305-8573, Japan*

[6] *PRESTO, Japan Science and Technology Agency, Kawaguchi, Saitama 332-0012, Japan*

[*] *These authors contributed equally to this work.*

(Dated: March 22, 2019)

Abstract

We have investigated the charge transport in the paramagnetic metallic phase of hole-doped pyrochlore iridates. The temperature dependence of thermopower shows a remarkable peak, typically 45 μV/K at 20 K, in a wide doping range from a heavily doped region to nearby the Mott transition. Calculations based on local density approximation and dynamical mean field theory show the presence of a quadratic band touching (QBT) in these compounds. This quantitatively elucidates the thermopower characteristics and specific heat of the doping induced metallic state, suggesting that the QBT is a common and robust feature in the paramagnetic metallic phase of hole-doped pyrochlore iridates even in the proximity of the Mott transition.

The interplay between relativistic spin-orbit interaction and electron correlation produces a fertile research field of strongly correlated topological semimetals. A remarkable example is the Dirac/Weyl semimetal, wherein massless or small effective-mass electrons give rise to unusual charge transport due to the non-trivial Berry phase[1–3]. The pyrochlore-type iridates $R_2Ir_2O_7$ (R =rare earth elements) are candidates of strongly correlated Weyl semimetals, which offers a unique opportunity to study the Mott physics of Weyl electrons[4–7]. Recent theoretical studies have clarified the possible emergence of antiferromagnetic Weyl semimetallic phase nearby the Mott transition, wherein Weyl points as well as the metallic edge state are topologically guaranteed by the broken time reversal symmetry due to the antiferromagnetic order. Indeed, signatures of the Weyl semimetallic phase such as the enhanced anomalous Hall effect as well as the metallic edge state emerging at the antiferromagnetic domain wall have been observed[8–12]. In fact, the Weyl semimetallic phase of $R_2Ir_2O_7$ is fragile at zero magnetic field and is limited to a narrow range below the antiferromagnetic transition temperature [Fig. 1(a)], whereas it extends to a wider temperature area under the magnetic field[16].

In the context of correlated Weyl semimetals, there is a growing interest in another semimetallic state, which is characterized by a touching of two parabolic bands at a discrete point in momentum space as illustrated in Fig. 1 (b). For these compounds, the band touching (quadratic band touching, QBT) at the Γ-point is guaranteed by the cubic crystal symmetry and the time-reversal symmetry, and thus should be robust against perturbations which keep these symmetries intact. Historically, the QBT has been recognized in some zero-gap semiconductors such as α-Sn[17], and was recently identified for $Pr_2Ir_2O_7$, which is a paramagnetic semimetal in the proximity to the metal-insulator transition [Fig. 1 (a)][18,19]. It has been theoretically proposed that electronic correlation effect in combination with the QBT causes non-Fermi liquid behavior with anomalous charge transport and dielectric/magnetic susceptibility[20–23]. Indeed, signatures of unusual magnetic and optical response have been reported by measurements of the magnetic Gruneisen number and terahertz optical spectrum in $Pr_2Ir_2O_7$[24,25]. In this context, $R_2Ir_2O_7$ is expected to offer an interesting opportunity to study the QBT in the strongly correlated region nearby the Mott transition, but the interplay between the QBT and the electron correlation has remained to be elusive. In this paper, by means of thermoelectric measurements and theoretical calculations, we propose that the QBT robustly subsists against the modest changes of one-electron

band-width and/or band-filling in the paramagnetic phase of $R_2Ir_2O_7$. Remarkably, our results suggest that the QBT reemerges by doping the Mott insulating phase, wherein the band structure with the QBT is destroyed by strong electron correlations. Specifically, the QBT is likely to give rise to a thermopower peak as large as 40 μV/K around 20 K by tuning the one-electron band-width or band-filling.

The densely-packed polycrystalline samples with large-size grains (1-10 μm) of $(Eu_{1-x}Ca_x)_2Ir_2O_7$, $[(Nd_{0.2}Pr_{0.8})_{1-x}Ca_x]_2Ir_2O_7$ and $(Pr_{1-x}Ca_x)_2Ir_2O_7$ were synthesized under 3 GPa and at 1200 °C by using the cubic-anvil-type furnace. The cubic crystal symmetry enables us to perform the precise resistivity, magnetization, specific heat and thermoelectric measurements. The results of powder x-ray diffraction show that all the samples were of a single phase that keeps the cubic crystal symmetry. The lattice constant of the Ca-doped compounds satisfies Vegard's law (Fig. S1 in the Supplementary Material[26]). The resistivity and specific heat were measured by the four-probe method and relaxation method, respectively. The magnetization was measured by means of a superconducting quantum interference device (SQUID) at 0.01 T.

In $R_2Ir_2O_7$, the one-electron band-width and band-filling of Ir 5d-state can be finely controlled by chemical substitution on the R-ion site. The effective one-electron band-width increases with decreasing the lattice distortion as measured by the Ir-O-Ir bond angle distortion via increasing the average ionic radius of R-ion. Furthermore, the band-filling can be controlled by hole doping via partial substitution of the trivalent R-ion with the divalent Ca-ion. As demonstrated in Fig. 1(a), the transition temperature (T_N) of antiferromagnetic insulating phase with all-in all-out magnetic ordering is smoothly reduced by changing the R-ions from Eu to Nd and vanishes at R=$Nd_{0.2}Pr_{0.8}$; the insulator-metal transition is driven by the electron correlation, resulting in the quantum Mott transition[13–15]. The Weyl semimetallic state shows up in the narrow temperature range immediately below the antiferromagnetic transition and yields a sizable anomalous Hall effect stemming from the Berry curvature accompanying the tiny net magnetization (a few mμ_B/f.u.)[8]. In fact, such a sizable anomalous Hall effect is one of the important signatures of the Weyl semimetal phase.

This stands in contrast with the case of the QBT in the paramagnetic phase; the transport signature to detect the QBT has been barely understood. Here, we found that the presence of QBT is supported by a characteristic peak in the temperature dependence of

the Seebeck coefficient (S). Figure 1 (c) shows the temperature dependence of S calculated for a single QBT with isotropic band dispersion as illustrated in Fig. 1 (b). We calculated S in the scheme of the standard Boltzmann transport theory, assuming an energy independent relaxation time and the symmetric dispersion for conduction- and valence-bands for brevity. S shows a peak at a temperature corresponding to the half of Fermi level ($E_{\rm F}/2$), and thus the peak shifts to higher temperature with decreasing $E_{\rm F}$ below the energy of QBT. In a straightforward picture, the peak can be understood from the balance between the electron and hole contributions; the contribution of hole is dominant at low temperatures, while the contribution of thermally excited electrons partially cancels the former at sufficiently high temperatures. In the present model, the peak value does not depend on $E_{\rm F}$ and the band mass. The latter feature can be understood from the fact that S does not depend on A for the band dispersion $E(\mathbf{k}) = A|\mathbf{k}|^n$ in the scheme of Boltzmann transport theory with a natural number n[27].

A similar peak feature in the temperature dependence of S can be seen in $(Pr_{1-x}Ca_x)_2Ir_2O_7$ and $[(Nd_{0.2}Pr_{0.8})_{1-x}Ca_x]_2Ir_2O_7$. Note that the latter is located on the verge of the quantum Mott transition as shown in Fig. 1(a), but remains to be a paramagnetic metal down to low temperatures (Fig. S2 in the Supplementary Material[26]). Figures 1(d) and (e) show the temperature dependence of S for both series of materials. For x=0 and 0.01, the sign of S is negative at high temperatures and a dip is observed for $50-100$ K. With increasing x, the dip is smeared out, and a peak gradually grows around 30 K for heavily doped systems. Notably, S reaches 45 μV/K at 23 K for $(Pr_{1-x}Ca_x)_2Ir_2O_7$ with $x = 0.05$, which is comparable with the typical thermoelectric oxide $NaCo_2O_4$[28]. A similar behavior is observed for $[(Nd_{0.2}Pr_{0.8})_{1-x}Ca_x]_2Ir_2O_7$ with $x = 0.05$ as shown in Fig. 1(e). The peak value appears to be nearly x-independent for $x > 0.05$, whereas the peak shifts to higher temperatures with increasing x. Figures 2 (a) and 2 (b) show the peak value (S^*) and peak temperature (T^*) for both series of compounds plotted as a function of x. Both series show the common feature that S^* steeply increases in the lightly doped region ($x \leq 0.05$), but is less x-dependent in a heavily doped region ($x \geq 0.05$) with a value of approximately 45 μV/K. On the other hand, it is evident that T^* monotonically increases as x increases in a heavily doped region, while it shows a rather complicated behavior for $x < 0.02$. Such a thermopower peak at low temperature reminds us of the phonon-drag effect as often observed in metals or semiconductors. However, the characteristic temperature

of a peak due to the phonon-drag effect is determined by the Debye temperature and thus is not consistent with the significant increase of T^* as a function of x in the present case. A more plausible scenario is the aforementioned mechanism by the QBT. Although we could not exclude the possibility of a small gap-opening with the magnitude of a few meV, given that the crystal symmetry remains to be cubic, it is most likely that the QBT subsists and governs the thermoelectric response even in the doped metallic phase. We anticipate that the modest x-dependence of the peak value in the heavily doped region originates from a deviation of low-energy band structure from a simple QBT and/or the energy dependent relaxation time (see below). On the other hand, the coexistence of a peak and profound dip in the lightly doped region ($x < 0.02$) cannot be understood by the aforementioned model; the complicated behavior may be attributed to an energy dependent relaxation time.

Next, we explored whether the temperature dependence of S can be universally seen even in the metallic phase obtained by hole-doping a Mott insulating parent compound ($x = 0$). Figure 3 (a) shows the temperature dependence of the resistivity for $(Eu_{1-x}Ca_x)_2Ir_2O_7$. The resistivity shows an insulating behavior with a kink at T_N (= 123 K) for the parent compound $Eu_2Ir_2O_7$ (x=0), and gradually decreases with increasing x while keeping the kink for $x \leq 0.03$. For $x \geq 0.05$, the metallic behavior subsists down to 2 K, and the signature of antiferromagnetic transition is no longer clear. Figure 3 (b) shows the temperature dependence of the magnetization for $(Eu_{1-x}Ca_x)_2Ir_2O_7$. The antiferromagnetic transition manifests itself as an upturn of the magnetization and is discernible up to $x = 0.05$. It is evident that both T_N and the magnetization at 2 K decrease with increasing x. The electronic phase diagram of $(Eu_{1-x}Ca_x)_2Ir_2O_7$ is summarized in Fig. 3 (c). T_N is suppressed with increasing x and appears to vanish around $x = 0.05$ accompanied by the doping induced (band-filling controlled) metal-insulator transition. We note that the signature of Weyl semimetallic phase has not yet been detected for the present compound in contrast to the case of $(Nd_{1-x}Pr_x)_2Ir_2O_7$ which features a band-width controlled metal-insulator transition. The metal-insulator transition can also be quantified by the electronic specific heat coefficient (γ). Here, γ is derived by the extrapolation of the specific heat divided by temperature (C/T) plotted as a function of T^2 to zero temperature (Fig. S3 in the Supplementary Material[26]). As shown in Fig. 3 (c), γ rapidly grows above $x = 0.04$ and exceeds 20 mJ/mol K^2 for $x = 0.05$, suggesting the emergence of a sizable Fermi surface. We note that a similar value has been observed for $(Y_{1-x}Ca_x)_2Ir_2O_7$[29]. As shown in Fig.

3 (d), S shows a peak consistent with the QBT feature in a wide doping range. Similarly to the case of $(Pr_{1-x}Ca_x)_2Ir_2O_7$ and $[(Nd_{0.2}Pr_{0.8})_{1-x}Ca_x]_2Ir_2O_7$, S^* is nearly x-independent $(22-30\mu V/K)$, while T^* monotonically increases as x increases. Indeed, as shown in Fig. 2 (a) and 2 (b), T^* of $(Eu_{1-x}Ca_x)_2Ir_2O_7$ nearly coincides with those for $(Pr_{1-x}Ca_x)_2Ir_2O_7$ and $[(Nd_{0.2}Pr_{0.8})_{1-x}Ca_x]_2Ir_2O_7$, whereas S^* is slightly smaller for the former. These results suggest that the QBT is realized even in the doping induced paramagnetic phase of $(Eu_{1-x}Ca_x)_2Ir_2O_7$.

In order to substantiate the existence of the QBT in the doping induced paramagnetic phase, we performed the band calculation on the basis of local density approximation (LDA) combined with dynamical mean field theory (DMFT). In the LDA calculation, the renormalization effect on the level of random phase approximation is included by using the modified Becke-Johnson exchange potential[30–35]. Figure 4 (a) shows the band structure for $(Eu_{1-x}Ca_x)_2Ir_2O_7$ with x=0.1 calculated by LDA as well as that calculated by LDA + DMFT with the Hubbard interaction U = 1.3 eV. Here, the LDA result is rescaled by an additional renormalization factor z=0.15 in order to highlight similarities to the LDA + DMFT spectral function. Note that the LDA + DMFT spectral function is obtained by introducing a small energy broadening. Both results are nearly identical in the vicinity of E_F as confirmed by a Fermi liquid-like self-energy. Small differences arising from the discretization in the course of DMFT using the exact diagonalization method appear below -0.05 eV and above 0.05 eV. However, the thermal transport is predominated by a small energy window (of $\pm\ 4k_BT$) around E_F. Therefore, the thermopower at low temperatures *e.g.* below about 150 K, will not be strongly affected by these small differences[27]. In the DMFT calculation, we considered only j_{eff} = 1/2-state, omitting j_{eff} = 3/2-state, because the LDA results show no direct crossing between the j_{eff} = 1/2-state and j_{eff} = 3/2-state. The renormalized j_{eff} = 1/2-state lies between -0.075 to 0.05 eV, whereas the renormalized j_{eff} = 3/2-state is located below -0.05 eV. Our result suggests that the QBT emerges at the Γ-point similar to the case of $Pr_2Ir_2O_7$[5,19,21]. The QBT is located at 10 meV above E_F as expected from the hole doping. We note that the band dispersion is sizable along the $\Gamma - X$ line, but is significantly flattened along the $\Gamma - L$ line, This is consistent with the previous calculations for $Y_2Ir_2O_7$[37]. We have calculated γ on the basis of the LDA +DMFT results. The calculated value is 29 ± 3 mJ/Ir mol K^2, which quantitatively agrees with the experimental result (= 26 mJ/Ir mol K^2).

Furthermore, we calculated S on the basis of the LDA + DMFT spectra by employing the quantum many-body Kubo formalism[26,36]. Figure 4 (b) shows the calculated temperature dependence of S. Both the LDA with $z = 0.15$ and LDA + DMFT ($U = 1.3$ eV) results show a peak structure as observed in the experimental result at low temperatures. The LDA + DMFT results are in good quantitative agreement with the experiment, while the renormalized LDA results give larger peak value and peak temperature. Although the value of S calculated with the LDA+DMFT depends on the choice of the broadening factor, the results robustly show a presence of a peak in S, which is governed by the QBT even with anisotropic band dispersion. The nearly dispersionless part along $\Gamma - L$ line gives rise to the enhanced density of states above $E_{\rm F}$, but merely gives less contribution to S due to the small Fermi velocity. Finally, we remark the thermally induced sign change of S at high temperatures, which is commonly observed in most of the samples. At high temperatures, the renormalized LDA results show the same behavior as the simple model in Fig. 1(b); S decreases but always remains positive. We note that the LDA +DMFT spectral function for $T > 190$ K does not feature a quasiparticle resonance. Generally, for hole-doped Mott insulators at high temperatures within the DMFT, the thermal fluctuation suppresses quasiparticles and only incoherent spectral weight remains in the vicinity of $E_{\rm F}$. Thus, all-band structure of the $j_{\rm eff} = 1/2$-state contributes to S, and the asymmetry of the local spectral function dominates the sign of S. Here, consistently with the experimental results, S of the LDA + DMFT becomes negative.

In summary, we report the charge transport measurements for hole-doped pyrochlore iridates $R_2Ir_2O_7$ (R=Pr, Nd and Eu). These compounds show an enhanced thermopower peak, typically reaching 45 μV/K at 20 K, in a wide doping range of paramagnetic metallic phase. Specifically, the metallic phase with such a characteristic thermopower peak can be induced even from the Mott insulating phase by hole-doping. Combined with the elaborate calculations based on local density approximation and dynamical mean field theory, we have provided the evidence that a quadratic band touching (QBT) emerges in the doping-induced paramagnetic metallic phase, resulting in the characteristic temperature dependence of the thermopower as observed in the experiment. These results suggest that the topologically protected character of QBT is robust even in the strongly correlated electron system nearby the Mott transition, which opens a way to create the Weyl semimetallic phase on the verge of filling-controlled Mott transition in this class of material.

We thank Y. Motome for useful discussions. This work was partly supported by Grant-In-Aid for Science Research (Nos. 16H00981, 18H01171, 18H04214, 16H06345) from the MEXT, and by PRESTO(No. JPMJPR15R5) and CREST(No. JPMJCR16F1), JST, Japan.

[1] J. Xiong, S. K. Kushwaha, T. Liang, J. W. Krizan, M. Hirschberger, W. Wang, R. J. Cava, and N. P. Ong, Science **350**, 413 (2015).

[2] M. Hirschberger, S. Kushwaha, Z. Wang, Q. Gibson, S. Liang, C. A. Belvin, B. A. Bernevig, R. J. Cava, and N. P. Ong, Nat. Mater. **15**, 1161 (2016).

[3] P. J. W. Moll, N. L. Nair, T. Helm, A. C. Potter, I. Kimchi, A. Vishwanath, J. G. Analytis, Nature **535**, 266 (2016).

[4] X. Wan, A. M. Turner, A. Vishwanath and S. Y. Savrasov Phys. Rev. B 83, 205101 (2011).

[5] W. Witczak-Krempa and Y. B. Kim *Phys. Rev. B.* **85**, 045124 (2012).

[6] W. Witczak-Krempa, G. Chen, Y. B. Kim and L. Balents, Annu. Rev. of Condens. Matter Phys. 5, 57 (2014).

[7] K. Ueda, J. Fujioka, Y. Takahashi, T. Suzuki, S. Ishiwata, Y. Taguchi, and Y. Tokura, *Phys. Rev. Lett.* **109**, 136402 (2012).

[8] K. Ueda, R. Kaneko, H. Ishizuka, J. Fujioka, N. Nagaosa, and Y. Tokura, *Nature Commun.* **9**, 3032 (2018).

[9] K. Ueda, J. Fujioka, Y. Takahashi, T. Suzuki, S. Ishiwata, Y. Taguchi, M. Kawasaki and Y. Tokura *Phys. Rev. B.* **89**, 075127 (2014).

[10] E. Y. Ma Y. T. Cui, K. Ueda, S. Tang, K. Chen, N. Tamura, P. M. Wu, J. Fujioka, Y. Tokura, Z. X. Shen, Science 350, 538 (2015).

[11] Y. Yamaji and M. Imada, *Phys. Rev. X* **4**, 021035 (2014).

[12] R. Schaffer, E. Kin-Ho Lee, B.-J. Yang, and Y. B. Kim, *Rep. Prog. Phys.* 79, 094504 (2016).

[13] D. Yanagishima and Y. Maeno, J. Phys. Soc. Jpn. **70**, 2880 (2001).

[14] K. Matsuhira, M. Wakeshima, Y. Hinatsu and S. Takagi, J. Phys. Soc. Jpn. **80**, 094701 (2011).

[15] K. Ueda, J. Fujioka, C. Terakura and Y. Tokura, *Phys. Rev. B.* **92**, 121110(R) (2015).

[16] K. Ueda, T. Oh, B.-J. Yang, R. Kaneko, J. Fujioka, N. Nagaosa, and Y. Tokura, *Nature Commun.* **8**, 15515 (2017).

[17] S. Groves and W. Paul, *Phys. Rev. Lett.* **11**, 194 (1963).

[18] S. Nakatsuji, Y. Machida, Y. Maeno, T. Tayama, T. Sakakibara, J. van Duijn, L. Balicas, J. N. Millican, R. T. Macaluso, and Julia Y. Chan, *Phys. Rev. Lett.* **96**, 087204 (2006).

[19] T. Kondo M. Nakayama, R. Chen, J. J. Ishikawa, E.-G. Moon, T. Yamamoto, Y. Ota, W. Malaeb, H. Kanai, Y. Nakashima, Y. Ishida, R. Yoshida, H. Yamamoto, M. Matsunami, S. Kimura, N. Inami, K. Ono, H. Kumigashira, S. Nakatsuji, L. Balents and S. Shin *Nature Commun.* **6**, 10042 (2015).

[20] A. A. Abrikosov and S. D. Beneslavski *Sov. Phys. JETP* **32**, 699 (1971).

[21] E.-G. Moon, C. Xu, Y. B. Kim, and L. Balents, *Phys. Rev. Lett.* **111**, 206401 (2013).

[22] L. Savary, E.-G. Moon, and L. Balents, *Phys. Rev. X.* 4, 041027 (2014).

[23] I. Boettcher and I. F. Herbut, *Phys. Rev. B.* **95**, 075149 (2017).

[24] Y. Tokiwa, J. J. Ishikawa, S. Nakatsuji and P. Gegenwart, Nature Materials 13, 356 (2014).

[25] B. Cheng, T. Ohtsuki, D. Chaudhuri, S. Nakatsuji, M. Lippmaa and N. P. Armitage, Nature Commun. 8, 2097 (2017).

[26] See Supplemental Material for additional information on structural parameter, resistivity, specific heat and theoretical calculations, which includes References.

[27] H. Usui and K. Kuroki, *J. Appl. Phys.* **121**, 165101 (2017).

[28] I. Terasaki, Y. Sasago and K. Uchinokura, *Phys. Rev. B.* **56**, R12685 (1997).

[29] H. Fukazawa and Y. Maeno *J. Phys. Soc. Jpn* **71**, 2578 (2002).

[30] F. Tran and P. Blaha *Phys. Rev. Lett.* **102**, 226401 (2009).

[31] D. Koller, F. Tran and P. Blaha *Phys. Rev. B.* **85**, 155109 (2012).

[32] P. Blaha, K. Schwarz, G. K. H. Madsen, D. Kvasnicka, J. Luitz, R. Laskowski, F. Tran and L. D. Marks, http://www.wien2k.at.

[33] J. Kunes, R. Arita, P. Wissgott, A. Toschi, H. Ikeda and K. Held, Comput. Phys. Commun. 181, 1888 (2010).

[34] A. A. Mostofi et al., Comput. Phys. Commun. 178, 685 (2008).

[35] A. Georges, G. Kotliar, W. Krauth and M. J. Rozenberg, Rev. Mod. Phys. 68, 13 (1996).

[36] K. Held, R. Arita, V. I. Anisimov, K. Kuroki, *Properties and Applications of Thermoelectric Materials* Springer (2009) pp. 141-157.

[37] H. Shinaoka, S. Hoshino, M. Troyer and P. Werner *Phys. Rev. Lett.* **115**, 156401 (2015).

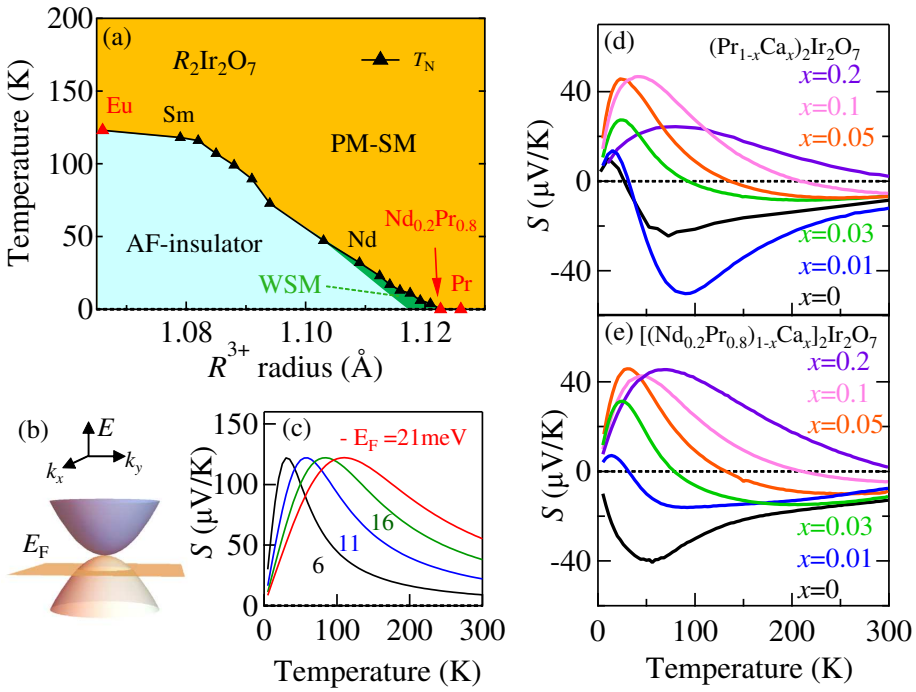

FIG. 1: (a) The electronic phase diagram of $R_2Ir_2O_7$ (R=Eu, Sm, Nd and Pr) and their solid solution. The triangles denote the transition temperature of antiferromagnetic (AF) ordering T_N[13–15]. The green region below T_N denotes the Weyl semimetallic (WSM) phase. (b) The illustration of quadratic band touching (QBT). The plane denotes the position of Fermi energy (E_F) as measured from the position of the band touching. The energy of QBT is defined as zero. (c) The Seebeck coefficient S calculated by the simple model assuming a single QBT as illustrated in (b). Here, we fix the energy dependence of relaxation time for brevity. In reality, the peak value can depend on E_F due to the change of profile of relaxation time. The temperature dependence of Seebeck coefficient (d) for $(Pr_{1-x}Ca_x)_2Ir_2O_7$ and (e) for $[(Nd_{0.2}Pr_{0.8})_{1-x}Ca_x]_2Ir_2O_7$.

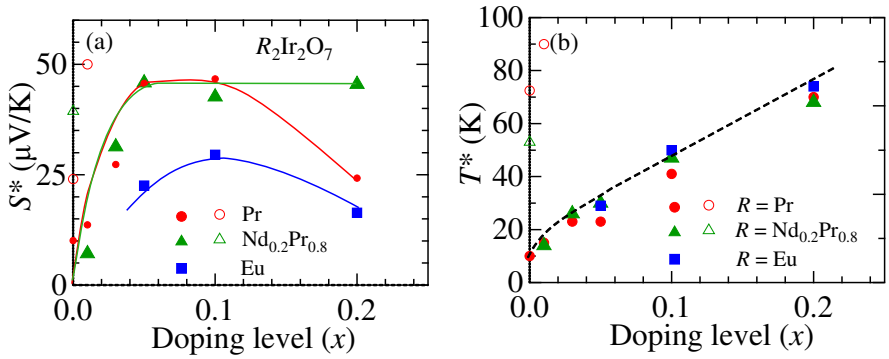

FIG. 2: (a) The peak/dip value of S and (b) the peak temperature of S as a function of x. The circle, triangle and square indicate results for $(Pr_{1-x}Ca_x)_2Ir_2O_7$, $[(Nd_{0.2}Pr_{0.8})_{1-x}Ca_x]_2Ir_2O_7$ and $(Eu_{1-x}Ca_x)_2Ir_2O_7$, respectively. The closed (open) symbol corresponds to the peak (dip) of Seebeck coefficient. The solid and dashed lines are shown by the guide to the eye.

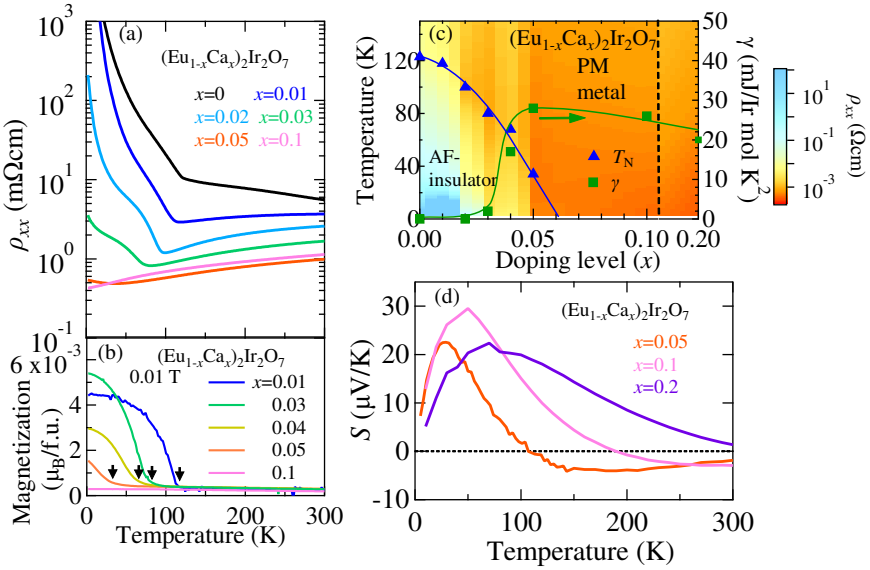

FIG. 3: Temperature dependence of (a) resistivity and (b) magnetization for $(Eu_{1-x}Ca_x)_2Ir_2O_7$. Arrows denote the transition temperature of antiferromagnetic ordering T_N. (c) The contour map of resistivity in the x-T plane as well as the x-dependence of T_N and γ for $(Eu_{1-x}Ca_x)_2Ir_2O_7$. T_N and γ are denoted by triangle and square, respectively. The solid line is shown by the guide to the eye. (d) Temperature dependence of the Seebeck coefficient for $(Eu_{1-x}Ca_x)_2Ir_2O_7$.

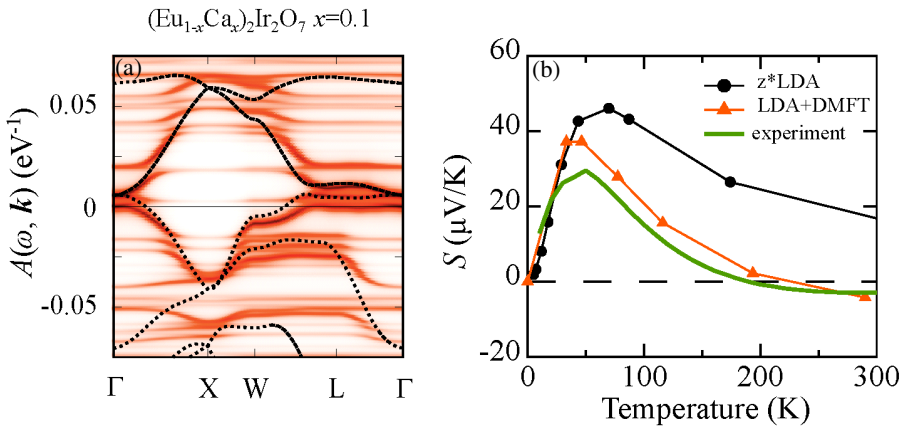

FIG. 4: (a) The band structure calculated by the LDA + DMFT ($U = 1.3$ eV) for the paramagnetic metallic phase of $(Eu_{1-x}Ca_x)_2Ir_2O_7$ with x=0.1. The temperature is set at 33 K. The black line denotes the LDA result with the renormalization factor z=0.15. (b) Calculated Seebeck coefficient on the basis of the band structure by LDA (circle) and LDA + DMFT (triangle).